Coercive Fields Above 6 T in Two Cobalt(II)-Radical Chain Compounds

Liu, Xiaoqing; Feng, Xiaowen; Meihaus, Katie R.; Meng, Xixi; Zhang, Yuan; Li, Liang; Liu, Jun-Liang; Pedersen, Kasper Steen; Keller, Lukas; Shi, Wei

Total number of authors:
13

Published in:
Angewandte Chemie International Edition

Link to article, DOI:
10.1002/anie.202002673

Publication date:
2020

Document Version
Peer reviewed version

Title: Coercive Fields Above 6 T in Two Cobalt(II)-Radical Chain Compounds

Authors: Wei Shi, PhD; Xiaoqing Liu; Xiaowen Feng; Katie R. Meihaus; Xixi Meng; Yuan Zhang; Liang Li; Jun-Liang Liu; Yi-Quan Zhang; Peng Cheng; Jeffrey R. Long

To be cited as: 10.1002/anie.202002673

Link to VoR: https://doi.org/10.1002/anie.202002673

Coercive Fields Above 6 T in Two Cobalt(II)-Radical Chain Compounds

Xiaoqing Liu,[+] Xiaowen Feng,[+] Katie R. Meihaus,[+] Xixi Meng, Yuan Zhang, Liang Li, Jun-Liang Liu, Wei Shi,* Yi-Quan Zhang, Peng Cheng,* and Jeffrey R. Long*

[*] Dr. X. Liu,[+] X. Meng, Y. Zhang, L. Li, Prof. Dr. W.Shi, Prof. Dr. P. Cheng
College of Chemistry
Key Laboratory of Advanced Energy Materials Chemistry (MOE), Nankai University, Tianjin 300071, China
E-mail: shiwei@nankai.edu.cn; pcheng@nankai.edu.cn
Dr. X. Feng,[+] Dr. K. R. Meihaus,[+] Prof. Dr. J. R. Long
Department of Chemistry, University of California, Berkeley, CA 94720, USA
E-mail: jrlong@berkeley.edu
Prof. Dr. J.-L. Liu
Key Laboratory of Bioinorganic and Synthetic Chemistry of Ministry of Education, School of Chemistry, Sun Yat-Sen University, Guangzhou 510275, China
Prof. Dr. Y.-Q. Zhang
Jiangsu Key Laboratory for NSLSCS, School of Physical Science and Technology, Nanjing Normal University, Nanjing 210023, China
Prof. Dr. J. R. Long
Department of Chemical and Biomolecular Engineering, University of California, Berkeley, CA 94720, USA
E-mail: jrlong@berkeley.edu
Prof. Dr. J. R. Long
Materials Sciences Division, Lawrence Berkeley National Laboratory, Berkeley, CA 94720, USA
E-mail: jrlong@berkeley.edu
[+] These authors contributed equally to this work.

Supporting information for this article can be found under: xxx

Abstract: Lanthanide permanent magnets are widely used in applications ranging from nanotechnology to industrial engineering. However, limited access to the rare earths and rising costs associated with their extraction are spurring interest in the development of lanthanide-free hard magnets. Zero- and one-dimensional magnetic materials are intriguing alternatives due to their low densities, structural and chemical versatility, and the typically mild, bottom-up nature of their synthesis. Here, we present two one-dimensional cobalt(II) systems $Co(hfac)_2$(R-NapNIT) (R-NapNIT = 2-(2′-(R-)naphthyl)-4,4,5,5-tetramethylimidazoline-1-oxyl-3-oxide, R = MeO or EtO) supported by air-stable nitronyl nitroxide radicals. These compounds are single-chain magnets and exhibit wide, square magnetic hysteresis below 14 K, with giant coercive fields up to 65 or 102 kOe measured using static or pulsed high magnetic fields, respectively. Magnetic, spectroscopic, and computational studies suggest that the record coercivities derive not from three-dimensional ordering but from the interaction of adjacent chains that compose alternating magnetic sublattices generated by crystallographic symmetry.

Introduction

The late 20th century witnessed the development of hard permanent magnets such as $Nd_2Fe_{14}B$ and $SmCo_5$, which are now widely used in diverse applications including in high-density information storage, magnetic resonance imaging, and electric motors. A key physical characteristic of such materials is their ability to retain a magnetized state in the absence of an applied field, a phenomenon that is exemplified in the form of a wide magnetic hysteresis loop.[1] Such a material can be permanently magnetized by application of a field and will only lose magnetization upon application of an opposing magnetic field of the appropriate strength, below a certain critical temperature. The magnetic field strength required to eliminate the magnetic polarization is known as the coercive field, H_c, and this parameter dictates the magnetic hardness of the material. A large H_c is essential for many applications, for example to protect high-density magnetic memory storage devices from information loss due to external perturbations. Importantly, increasing the magnetic hardness of a material can also reduce the quantity of the material required for a given application, which is highly valuable in environments where physical space is at a premium. The $Nd_{14}Fe_{80}B_6$ and $SmCo_5$ alloys exhibit large coercive fields of 39 kOe (at 77 K) and 43 kOe (at 4.2 K), respectively,[2] although these values can vary depending on the structural integrity of the materials, and the high temperatures used in the alloy preparation can introduce deleterious defects and grain boundaries that severely limit the intrinsic magnetic hardness.[3] Considering potential limits to the availability of the lanthanides, in contrast to a number of transition metals, as well as the increasingly negative environmental impacts inherent to lanthanide mining and extraction, interest is growing in the development of lanthanide-free hard magnets.

Over the past two decades, a number of molecules and one-dimensional chain compounds, known as single-molecule magnets[4] and single-chain magnets,[5] respectively, have been found to exhibit large magnetic anisotropies and spin correlations that give rise to magnetic bistability and, in many cases, magnetic hysteresis akin to bulk magnets. While the magnetization dynamics of these molecules[6] and chain compounds[7] share several key characteristics, one difference is that single-chain magnets will always exhibit magnetic hysteresis because intrachain exchange interactions preclude quantum tunneling of the magnetization. In addition, intrachain exchange interactions can engender strong magnetic moment

directionality along a chain, even in the absence of magnetically anisotropic lanthanide ions—which have alternatively played a key role in the development of single-molecule magnets exhibiting hysteresis at or near liquid nitrogen temperatures.[6d,6e] Chain compounds have thus received considerable attention as intriguing alternatives to lanthanide-free magnets.[4b] In single-chain magnets, magnetic hysteresis typically originates from the magnetization dynamics of the spin carriers along the chain, which are coupled by strong exchange interactions. This phenomenon was originally proposed by Glauber in 1963,[8] and was first demonstrated experimentally in 2001 with the discovery of the one-dimensional radical-bridged compound $Co(hfac)_2$(NITPhOMe) (NITPhOMe = 4′-methoxy-phenyl-4,4,5,5-tetramethylimidazoline-1-oxyl-3-oxide; or para-methoxyphenyl nitronyl nitroxide, *p*-C_1PNN), which has a coercive field of ~8 kOe at 2 K (3 kOe at 4.5 K).[5a] Single-chain magnet systems based on cobalt(II)-radical repeat units have since attracted considerable research interest.

In contrast to intrachain interactions, interchain magnetic interactions—often antiferromagnetic—were initially considered to be at odds with single-chain magnetism, as these could give rise to three-dimensional ordering.[9] However, it was discovered that single-chain magnetism could coexist or even compete with three-dimensional ordering arising from interchain interactions.[10] For example, single-chain magnets of the type $Co(hfac)_2$(*p*-C_nPNN) (*n* = 4, 5)[7b,11] and $Co(hfac)_2$(*o*-C_nPNN) (n = 2, 3, 5)[11,12] and [$Co(hfac)_2$]·BNO* (BNOH = 1,3-bis(N-tert-butyl-N-(oxylamino))benzene; BNO* = chiral triplet bis(nitroxide))[13] have been shown to exhibit three-dimensional ordering and wide magnetic hysteresis at low temperatures, with coercive fields as high as 52 and 54 kOe at 6 K for $Co(hfac)_2$(*p*-C_4PNN) and $Co(hfac)_2$(*o*-C_2PNN), respectively.[7b,11,12] These results highlighted that an interplay between single-chain magnet dynamics and intermolecular interactions that can lead to record-hard magnets;[14] for these systems, ordering was rationalized as arising from ferromagnetic[7b,7c,11,12] or antiferromagnetic[15] interactions. The development of one-dimensional materials with large correlation lengths that also exhibit suitable interchain interactions therefore stands as a worthwhile strategy for the design of new hard magnets. However, the relevance of the relative spatial orientations of neighboring chains in such systems has largely been overlooked, and despite active research within the last several years, no single-chain magnets have been identified that exhibit hard magnet properties surpassing the previous 54 kOe value for $Co(hfac)_2$(*o*-C_2PNN).[12] The realization of new systems is also in part rendered challenging by the weakly-coordinating character of the nitronyl nitroxide radical[5a,7b,7c,9b] and the complex nature of chain formation.

Here, we present detailed structural and magnetic characterization of two novel cobalt(II)-radical single-chain magnets $Co(hfac)_2$(R-NapNIT) (R-NapNIT = 2-(2′-(R-)naphthyl)-4,4,5,5-tetramethylimidazoline-1-oxyl-3-oxide, R = MeO and EtO) and investigate the role of chain orientation on coercivity. We also present the synthesis and characterization of the discrete, paramagnetic compounds $Co(hfac)_2(R\text{-NapNIT})_2$ (R = MeO and EtO), which represent units excised from the chains. Significantly, both one-dimensional compounds exhibit unprecedented large, square magnetic hysteresis at low temperatures, with coercive fields exceeding 60 kOe, surpassing all previous values measured for any bulk or single-chain magnet materials under a direct-current (dc) field. Structural analysis and ab initio calculations suggest that the interaction of two orientationally-distinct chains, and consequently magnetic sublattices, in each compound—in tandem with strong intrachain magnetic exchange—is critical to the large coercivity. To our knowledge, such dimorphism has not been identified previously as a determining factor in giving rise to large coercivity in single-chain magnets. We believe the design of similar dimorphic structures stands as an advantageous approach in the continued pursuit of lanthanide-free hard magnets.

Results and Discussion

The reaction of $Co(hfac)_2 \cdot 2H_2O$ with R-NapNIT (R = MeO and EtO) in a 1:2 molar ratio produces the discrete compounds **1** (R = MeO) and **2** (R = EtO) (Figure 1, upper) as black, microcrystalline solids. Alternatively, reactions of $Co(hfac)_2 \cdot 2H_2O$ and the respective radical ligands in a 1:1 ratio favor linking of these units through an additional $Co(hfac)_2$ moiety to yield the chain compounds **3** (R = MeO) and **4** (R = EtO) (Figure 1, lower), which form as black, microcrystalline solids with needle morphology. Single-crystal X-ray diffraction characterization revealed that **1** and **2** crystallize in the monoclinic *C*2/*c* space group, while **3** and **4** crystallize in the orthogonal $P2_12_12_1$ space group. All of the compounds exhibit a pseudo-octahedral cobalt(II) center coordinated by two cis R-NapNIT radicals and two hexafluoroacetylacetonate ligands. Semiquantitative polytopal analysis and continuous symmetry measurements of **1**–**4** indicated only minor differences in their cobalt(II) coordination environments (Figures S1 and Table S1). In **1** / **2** and **3** / **4**, the Co–O_{rad} bond lengths are 2.025(8) / 2.034(4) and 2.023(8) / 2.033(4) Å, respectively, the shortest distances reported to date for any cobalt(II)–nitronyl nitroxide radical compound (Figure S2a–b, Figure S3a–b, Table S2).[9a] These strong coordination bonds are supported by close hydrogen bonding contacts around the cobalt(II) centers (see Figures S2c–d and S3c–d) and are likely associated with the presence of strong cobalt(II)–radical magnetic coupling in all compounds.[5a,7b,7c] For compounds **3** and **4**, the shortest intrachain Co···Co distances are 7.512(5) and 7.557(4) Å, respectively, and adjacent chains are linked by C–H···F hydrogen bonds to form a three-dimensional supramolecular network with nearest interchain Co···Co distances of 10.487(1) and 10.537(6) Å for **3** and **4**, respectively (Figure S3e–f, Figure S4, Table S3).

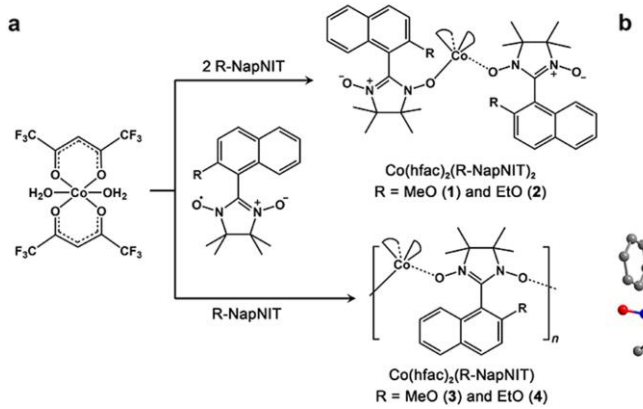

Figure 1. (a) Syntheses of compounds **1**–**4**. The reactions of $Co(hfac)_2 \cdot 2H_2O$ with R-NapNIT (R = MeO or EtO) in different molar ratios result in the formation of the mononuclear compounds **1** and **2** (1:2 ratio) and the chain compounds **3** and **4** (1:1 ratio). (b) Single-crystal X-ray diffraction structures of compounds **2** and **4**. Purple, red, blue, and gray spheres represent Co, O, N, and C atoms, respectively. Hydrogen atoms are omitted for clarity.

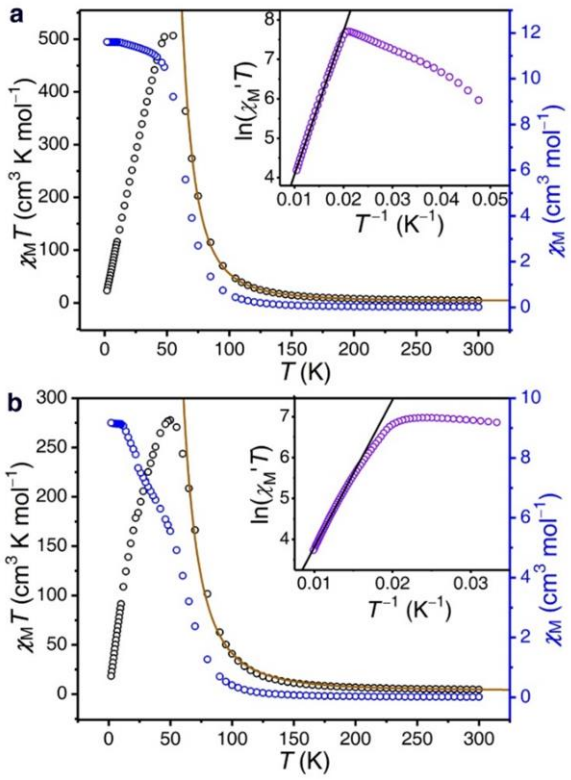

Figure 2. Variable-temperature molar magnetic susceptibility (χ_M) plots for **3** and **4**. χ_M (blue) and $\chi_M T$ (black) data collected for **3** (a) and **4** (b) under a 1000-Oe dc field for temperatures ranging from 2 to 300 K. The solid dark yellow lines correspond to fits to the data with J = −167±9 cm^{-1}, J_a = 168±8 cm^{-1}, D = −49±3 cm^{-1}, g_R = 2.00 (fixed), g_{Co} = 3.10±0.16, and k = 0.70 (fixed) for **3** and J = −157±8 cm^{-1}, D = −83±4 cm^{-1}, J_a = 156±7 cm^{-1}, g_R = 2.00 (fixed), g_{Co} = 3.11±0.16, and k = 0.70 (fixed) for **4**, as described in the text. Insets: Plots of $\ln(\chi_M'T)$ vs. T^{-1} under zero external field (where χ_M' is the real part of the ac susceptibility measured under zero dc field using a 3-Oe field oscillating at a frequency of 1 Hz). The solid black lines correspond to linear fits with Δ_ξ = 252±2 cm^{-1} and C_{eff} = 1.58±0.06 cm^3 K mol^{-1} for **3** and Δ_ξ = 250±2 cm^{-1} and C_{eff} = 1.25±0.04 cm^3 K mol^{-1} for **4**, as described in the text.

Static magnetic susceptibility data were collected using a direct current (dc) field of 0.1 T over the temperature range of 2–300 K to investigate magnetic exchange interactions in compounds **1**–**4**. At room temperature, the values of the molar magnetic susceptibility times temperature, $\chi_M T$, for the molecular species **1** and **2** are 1.40 and 1.48 cm^3 K mol^{-1}, both lower than the value of 2.62 cm^3 K mol^{-1} expected for an uncoupled, spin-only system,[16] especially considering a possible orbital contribution from octahedral, high-spin cobalt(II). These $\chi_M T$ values suggest the presence of strong intra- and/or intermolecular antiferromagnetic coupling of the radical–cobalt(II)–radical units, a supposition further supported by the rapid decline of $\chi_M T$ with decreasing temperature (Figures S6 and S7). Using the program PHI,[17] the $\chi_M T$ data were fitted with the Hamiltonian $\hat{H} = \mu_B B[g_R \cdot (\hat{S}_{R1} + \hat{S}_{R2}) + g_{Co} \cdot \hat{S}_{Co}] - 2J(\hat{S}_{R1} \cdot \hat{S}_{Co} + \hat{S}_{R2} \cdot \hat{S}_{Co})$, where J is the exchange-coupling constant between cobalt(II) and one radical and B is the magnetic field. Here, inter- and intramolecular coupling between radicals were assumed to be much weaker than J and therefore excluded from the Hamiltonian to avoid overparameterization.[7c] Intermolecular interactions (zJ') between the radical–cobalt(II)–radical units were modeled using the mean-field approximation. The resulting

fits afforded large negative values of J = −152±20 cm^{-1} and J = −133±8 cm^{-1} for **1** and **2**, respectively, indicative of very strong intramolecular antiferromagnetic cobalt–radical coupling, while g(Co^{2+}) / zJ' values of 2.84±0.34 / −10.3±1.3 cm^{-1} (**1**) and 2.39±0.34 / −23.3±3.7 cm^{-1} (**2**) fall within the range of values reported for other cobalt(II)–radical compounds.[18]

The room-temperature $\chi_M T$ values for **3** and **4** are 4.52 and 4.14 cm^3 K mol^{-1}, respectively, higher than the spin-only value of 2.25 cm^3 K mol^{-1} expected for a high-spin cobalt(II) and a radical in the absence of any exchange coupling (Figure 2). The magnitude of $\chi_M T$ can be ascribed to a significant orbital contribution from the octahedral cobalt(II) center and the ferrimagnetic spin arrangement along the chain. With decreasing temperature, the $\chi_M T$ product increases to maximum values of 506.44 and 304.18 cm^3 K mol^{-1} for **3** (at 55 K) and **4** (at 50 K), respectively, and then decreases to 23.20 and 16.87 cm^3 K mol^{-1} for **3** and **4**, respectively, at 2 K. Based on the similarity of the cobalt(II) coordination environments in **1**−**4**, strong intrachain magnetic coupling is also expected to occur in **3** and **4**. A fit to the $\chi_M T$ data for **3** above 65 K using the branch chain model[19] (see Supplemental Information, Section 1.3) yielded the parameters J = −167±9 cm^{-1}, D = −49±3 cm^{-1}, J_a = 168±8 cm^{-1}, g_R = 2.00 (fixed), g_{Co} = 3.10±0.16, and k = 0.70 (fixed) (Figure 2a), where D is the local anisotropy parameter for cobalt(II), J_a is the spin-orbit coupling parameter, and k is a fixed covalency factor. Likewise, the data for **4** were fit to obtain J = −157±8 cm^{-1}, D = −83±4 cm^{-1}, J_a = 156±7 cm^{-1}, g_R = 2.00 (fixed), g_{Co} = 3.11±0.16, and k = 0.70 (fixed) (Figure 2b). These large negative values of J support strong antiferromagnetic cobalt(II)–radical coupling in **3** and **4**, and the similarity of the coupling constants determined for **1**−**4** is consistent with the essentially congruent cobalt(II) coordination environments in these compounds.

For an anisotropic Heisenberg or Ising-like chain system, the product of the molar in-phase magnetic susceptibility (χ_M') times temperature increases exponentially with decreasing T, following the equation $\chi_M'T = C_{eff}\exp(\Delta_\xi/k_BT)$, where C_{eff} is the effective Curie constant and Δ_ξ is the correlation energy needed to create a domain wall within the chain. Accordingly, for a single-chain magnet, a plot of ln($\chi_M'T$) vs. 1/T should feature a linear region with positive slope corresponding to the correlation energy.[20] To investigate the one-dimensional magnetism of compounds **3** and **4**, variable-temperature alternating current (ac) susceptibility data were collected with a 3-Oe ac field oscillating at 1 Hz in the absence of a dc field. The resulting plots of ln($\chi_M'T$) vs. 1/T

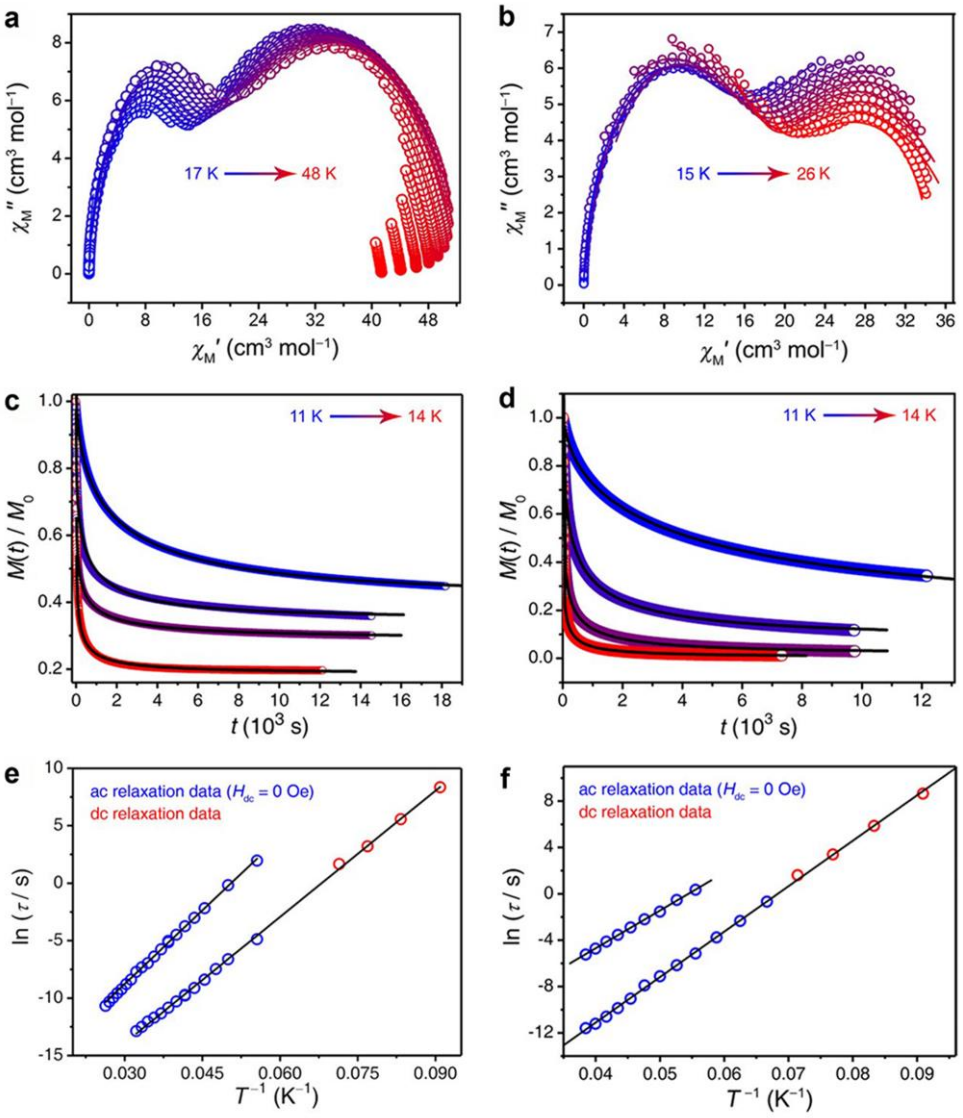

Figure 3. Dynamic magnetic data for **3** and **4**. Cole-Cole plots for **3** (a) and **4** (b). The solid lines represent fits using the generalized Debye model and/or a linear combination of two modified Debye models at the corresponding temperatures. Normalized dc magnetization vs. time decay plots for **3** (c) and **4** (d). The relaxation times at the indicated temperatures were obtained by fitting the data using the equation $M(t) = M_f + (M_0 - M_f)\exp[-(t/\tau)^\beta]$, where τ is the relaxation time, M_0 and M_f represent the initial and final magnetization values, respectively, and β can take on values ranging from 0 to 1.[4b] The solid lines correspond to the best fits. Plots of ln(τ) vs. T^{-1} obtained from the relaxation times extracted from ac and dc magnetic susceptibility measurements for **3** (e) and **4** (f). Solid lines represent fits of the data using the Arrhenius expression $\tau = \tau_0\exp(\Delta\tau/k_BT)$.

(Figure 2, insets) indeed feature a linear region of positive slope that confirms the one-dimensional nature of the magnetism in both chain compounds. The best fit to the linear data for **3** (from 52–96 K) and **4** (from 67–100 K) gave very high correlation energies of Δ_ξ = 252±2 cm^{-1} and 250±2 cm^{-1}, respectively, and corresponding C_{eff} = 1.58±0.06 and 1.25±0.04 cm^3 K mol^{-1}, respectively, indicating that the spins along the chain are strongly correlated by magnetic interactions and that the magnitudes of the magnetic interactions are similar for these two chains. The strong intrachain cobalt(II)−radical correlations in **3** and **4** further suggest that these materials would behave as

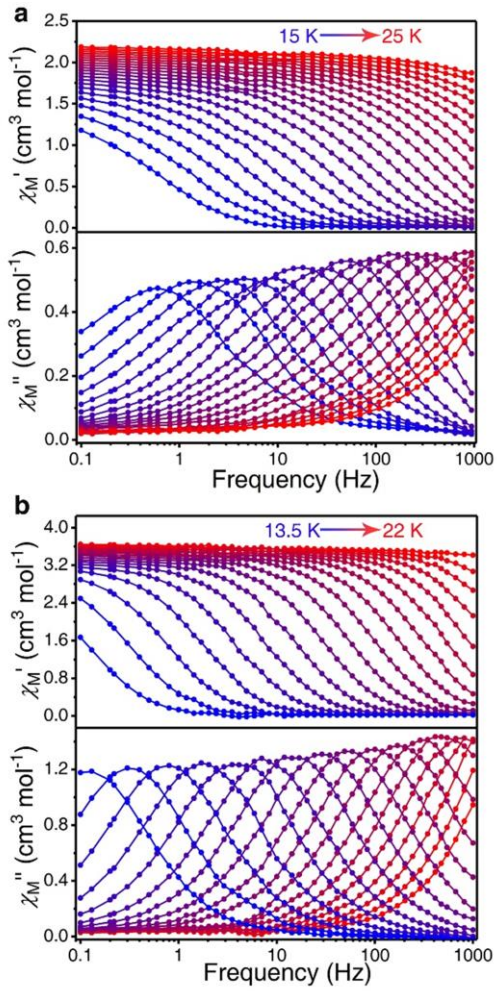

Figure 4. Ac magnetic susceptibility data collected for **3** and **4** under a dc field. Frequency dependence of the ac magnetic susceptibility under an optimum dc field of 550 Oe for **3** (a) and 500 Oe for **4** (b). Solid lines are guides for the eyes.

single-chain magnets with substantial energy barriers.

As a direct probe of the magnetization dynamics in **1**−**4**, variable-temperature ac magnetic susceptibility data were collected under zero dc field. No out-of-phase magnetic susceptibility (χ_M'') was observed for the molecular complexes **1** and **2** over the measured temperature and frequency range (Figures S8 and S9), indicating that any magnetization dynamics are faster than the timescale of the experiment. In contrast, the chain compounds exhibit both frequency- and temperature-dependent χ_M' and χ_M'' signals (Figures S10−S14). The ac magnetic susceptibility data for **3** and **4** (Figures S10 and S11) also clearly exhibit two features in χ_M'', namely a shoulder at low frequencies and a peak at intermediate frequencies, that are indicative of more than one relaxation process. In variable-temperature measurements, the χ_M' signal for **3** does not shift substantially with increasing frequency, and instead consistently reaches a maximum at ~46.5 K, suggestive of possible long-range magnetic ordering below this temperature (Figure S12). In contrast, the χ_M' signal for **4** shows is temperature-dependent and *shows no evidence of magnetic ordering*, gradually becoming broader with increasing frequencies with a shoulder at low temperatures (Figure S13). Two distinct peaks are present in the temperature-dependent χ_M'' data for **4**, again indicative of multiple relaxation processes (Figure S13). To exclude the possibility of spin glass behavior for **4**, we calculated the Mydosh parameter, φ, using the equation $\varphi = (\Delta T_p/T_p)/\Delta(\log\nu)$, where T_p corresponds to the maximum in χ_M'' for a given frequency ν.[21] For **4**, φ = 0.12, which is within the range typically observed for superparamagnetic systems (in contrast, 0.01 < φ < 0.08 for a spin glass).[21] Temperature-dependent relaxation times were extracted between 18 and 38 K for **3** and between 15 and 26 K for **4** by fitting Cole-Cole plots of χ_M' and χ_M'' using a generalized Debye model (Figures 3a−b and S15). For temperatures between 11 and 14 K for both **3** and **4**, the ac signal slows beyond the frequency range of the magnetometer, and thus the corresponding relaxation times were instead extracted from exponential fits of the time decay of the magnetization from dc relaxation measurements (Figure 3c−d).

The plots of the natural log of these combined relaxation times (Tables S4−S9) versus inverse temperature yielded two distinct, linear Arrhenius plots for each chain compound that were each fitted using the equation $\ln(\tau) = \ln(\tau_0) + \Delta_\tau(k_BT)^{-1}$ to extract energy barriers of Δ_τ = 297±6 and 254±4 cm^{-1} for **3** (with pre-exponential factors τ_0 = 4.2±1.3 × 10^{-10} and 1.5±0.4 × 10^{-11} s, respectively, see Figure 3e) and Δ_τ = 273±2 and 227±2 cm^{-1} for **4** (with τ_0 = 2.3±0.4 × 10^{-12} and 2.0±0.3 × 10^{-8} s, respectively, see Figure 3f), consistent with other values reported for single-chain magnets.[7c,9b] While one relaxation process is expected for relaxation along a single chain, coupling between neighboring chains could give rise to a second relaxation process.[5c] We note that this coupling could also result in a three-dimensional ordered phase that does not preclude single-chain magnetization dynamics,[10,22] which might explain the ordering observed for compound **3**. Indeed, this compound features a smaller substituent on the nitronyl nitroxide ligand and a smaller interchain distance than in **4**, which could facilitate stronger interchain interactions. The application of an external magnetic field can suppress interchain interactions, and thus, as a test of this hypothesis, we collected ac data under optimized dc fields of 550 and 500 Oe for **3** and **4**, respectively (Figure S16). Indeed, in these data, the low-frequency tails in χ_M'' are extinguished and single peaks are observed, indicative of pure single-chain magnetism (Figure 4). Arrhenius fits to the temperature-dependent relaxation data collected under these optimized dc fields yielded Δ_τ = 251±2 cm^{-1} / τ_0 = 9.1±1.8 × 10^{-12} s for **3** and Δ_τ = 254±2 cm^{-1} / τ_0 = 2.2±0.4 × 10^{-12} s for **4** (Figure S17). These energy barriers are among the highest reported for any single-chain magnets characterized to date.[7c,9b] In a single-chain magnet, the energy barrier arises from two contributions, namely the anisotropy energy from the molecular building unit (Δ_A) and the correlation energy from the magnetic coupling along the chain (Δ_ξ), and is described by $\Delta_\tau = \Delta_A + \Delta_\xi$ for a chain in the finite-size limit. Using this expression and values of Δ_ξ = 247±2

and 249±5 cm^{-1} for **3** and **4**, respectively (determined from fits of ln($\chi_M'T$) vs. 1/T data collected under the optimized dc fields, Figures S18 and S19), we determined Δ_A = 4 cm^{-1} for **3** and 5 cm^{-1} for **4**. Therefore, under a small optimized field, slow magnetic relaxation in **3** and **4** is dominated by one-dimensional correlation (intrachain magnetic coupling). These results also indicate that the dynamic behavior observed for **3** and **4** under zero dc field arises from a complex mixture of single-chain magnetization and significant interchain magnetic coupling.

Zero-field cooled (ZFC) and field-cooled (FC) magnetization data were collected for compounds **3** and **4** under an applied field of 100 Oe to further investigate the transition from a paramagnetic to a superparamagnetic/ordered state (Figures S20 and S21).[4b] With cooling, the ZFC/FC magnetization curves increase in magnitude and remain overlaid until ~46.5 and ~52.0 K for **3** and **4**, respectively, at which points the curves begin to level off and gradually diverge; a pronounced separation of the curves occurs at ~14 K for **3** or ~11 K for **4** as the ZFC magnetization drops to zero. The gradual divergence of the FC and ZFC curves is indicative of magnetic blocking, which can be correlated with the onset of magnetization relaxation of single-chain origin. The stark divergence of the FC and ZFC curves at ~14 K for **3** or ~11 K for **4** indicates an even more pronounced slowing of the magnetization relaxation at very low temperatures.

Zero-field powder neutron diffraction data were collected between 1.5 and 60 K (Figure S22) on a non-deuterated sample of **3** in an effort to investigate the nature of the magnetic ordering observed via ac susceptibility. Although the resulting normalized diffraction peaks were found to be consistent with the simulated peaks from the single-crystal X-ray diffraction data, indicating the high phase purity of the material, a high background signal precluded the observation of ordering.[23] We thus turned to specific heat measurements and collected data for **3** and **4** between 2 and 50 K under dc fields of 0, 0.1, and 1.0 T (Figures S23 and S24). No clear anomalies were identified in the data for the compounds; we ascribe this absence to a significant contribution of the lattice heat capacity, which can obscure signals arising from magnetic contributions. However, a peak becomes apparent for **3** at ~46.5 K when the zero-field heat capacity data is subtracted from the data collected under applied fields of 0.1 and 1 T (Figure S23, inset).[24] This anomaly is indicative of a phase transition around 46.5 K and is consistent with the in-phase magnetic susceptibility measurements, which indicated magnetic ordering in **3** at this same temperature. In contrast, no distinguishable anomaly is observed for **4** in the original curve or in the differential curve (Figure S24, inset), indicating the absence of a phase transition and consistent with the ac magnetic susceptibility data for this compound.

To probe the low-temperature magnetic behavior of **3** and **4**, we first performed field-dependent magnetization measurements between 2 and 14 K (Figures S25 and S26). Notably, the magnetization remains nearly zero at 2 K under an applied field as high as 4.0 T for **3** or 4.5 T for **4**, indicating a reasonably strong interaction between chains, despite an interchain separation of 10.487(1) Å for **3** and 10.537(6) Å for **4**. For **3**, between 2 and 7 K the magnetization follows the same trace and begins to increase steadily above 4 T, reaching a saturation value of 2.1 μB at 14 T. Between 9 and 14 K, the magnetization becomes temperature dependent and is saturated by a 7-T

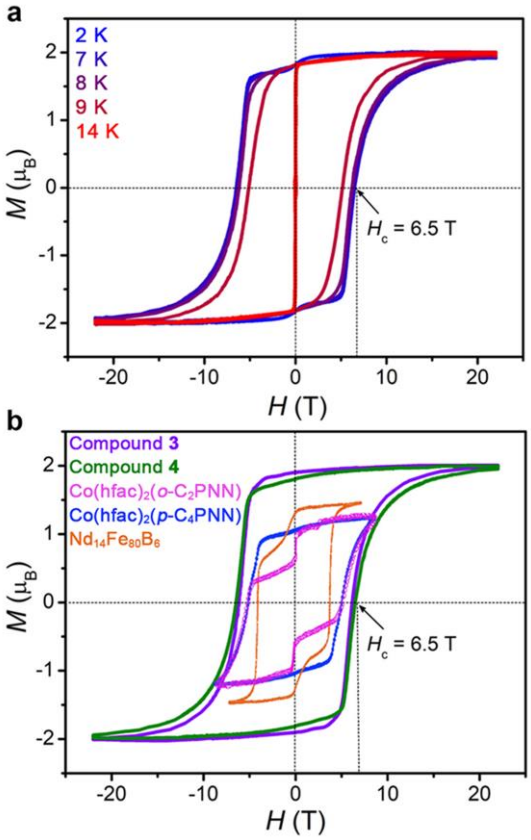

Figure 5. Magnetic hysteresis loops. Magnetic hysteresis data for **4** (a) and a comparison of magnetic hysteresis data for permanent magnets and select cobalt(II) radical chains: $Nd_{14}Fe_{80}B_6$ (77 K), Co(hfac)$_2$(o-C_2PNN) (6 K), Co(hfac)$_2$(p-C_4PNN) (6 K), **3** (7 K), **4** (7 K) (b). Data for **3** and **4** were collected using a sweep rate of 200 Oe/s.

magnetic field (Figure S25). For **4**, a similar magnetization process was observed (Figure S26).

Magnetization hysteresis loops were collected for **3** and **4** between ±7 or ±14 T in the temperature range of 2–14 K using a sweep rate of 100 Oe/s (Figures S27 and S28). Notably, both compounds exhibit substantial coercivity between 2 and 7 K, for example the coercive field of compound **3** is 59 kOe, although the magnetization of compound **4** does not saturated even as high as 14 T (Figure S28). We thus collected additional hysteresis data for both compounds (Figures 5a and S29) using continuous magnetic fields up to 25 T (sweep rate of 200 Oe/s) as well as pulsed magnetic fields up to 20 T (sweep rate of 433 T/s). Using continuous high fields between 2 and 7 K, we measured a giant coercive field of 62 kOe for compound **3** and 65 kOe for **4**. These values surpass the coercive fields of $Nd_{14}Fe_{80}B_6$ and $SmCo_5$ and the previous record of 54 kOe set by Co(hfac)$_2$(o-C_2PNN) (see Figure 5b). *To the best of our knowledge, the coercive field for **4** is the second highest for any one- or two-dimensional magnet* (H_c = 79 kOe at 10 K for the N_2^{3-} radical-bridged diterbium compound [K(crypt-222)][(Cp$^{Me4H}_2$Tb)$_2$(μ−$N_2^{\cdot}$)], measured using at a sweep rate of 100 Oe/s),[6c] and represents a record for any single-chain magnet (see Table S10).[5a,7b,7c,9a] The hysteresis loops measured using the pulsed magnetic fields (Figure S30) also showed an ultrahigh coercive field of 102 KOe, although this value is largely a consequence of the high sweep rate and low dimensional nature of the chain systems. Under all measurement conditions, the hysteresis loops for both compounds exhibit a very square shape. For example, at 7 K the ratio of the remanent magnetization to the saturation magnetization (M_r/M_s)[25] for **3** measured under a continuous field is 97%, while the ratio for **4** is 91% and 97% under continuous and pulsed high magnetic fields, respectively (Table S10). These results further indicate that the magnetic moments of the

chains are highly correlated in both **3** and **4**. For both chains, the coercive field decreases gradually with increasing temperature from 7 to 14 K, and the hysteresis loops are closed above 14 K.

We also collected hysteresis data for **3** and **4** at 2, 5, and 7 K using a sweep rate as low as 20 Oe/s, comparable to the 18 Oe/s sweep rate used to collect hysteresis data in the case of $Co(hfac)_2$(*o*-C_2PNN).[11] At 2 and 5 K, the coercive field is 59 kOe for **3** and 61 kOe for **4**, and these values decrease slightly to 57 and 60 kOe at 7 K, respectively (see Tables S11−S12). We note that this data was collected using a 7-T magnetometer, which would not normally saturate the chain compounds (see Figures S25 and S26). However, we were able to saturate the samples using this instrument and the following protocol at 2 K. Beginning at 15 K, a field of 7 T was applied and held while the temperature was subsequently decreased to 2 K; data was then collected as the field was decreased to −7 T. This process was then repeated in reverse starting from an applied field of −7 T. In this manner, the hysteresis data shown in Figures S31 and S32 could be obtained (and by extension, Figures S33−S36 for 5 and 7 K, respectively). *We propose that this method may be generally useful for collecting hysteresis data on compounds exhibiting hard magnet behavior, where the maximum accessible magnetic field with a given instrument may otherwise be a limitation.* Ultimately, such remarkable square hysteresis and the magnitude of the coercive field indicate a dramatic slowing down of the relaxation time for compounds **3** and **4** as the temperature is lowered below their critical temperatures.

Ab initio CASSCF/RASSI/SINGLE_ANISO calculations[26] were performed to compare and contrast the magnetic anisotropy in compounds **3** and **4** along with two other cobalt(II) chain compounds, $Co(hfac)_2$(PyrNN)[7c] (PyrNN = 2-(1′-pyrenyl)-4,4,5,5-tetramethylimidazoline-1-oxyl-3-oxide) and $Co(hfac)_2$(*p*-C_4PNN),[7b] which exhibit coercive fields of 32 kOe (at 8 K) and 52 kOe (at 6 K), respectively. The calculated magnetic axes of the cobalt(II) centers in all four compounds are visualized in Figure S37 and tabulated in Table S13.

The symmetry operations of the space group for each compound play an important role in the arrangement and packing of the chains and the orientations of their magnetic moments, which ultimately govern their magnetic properties. The chain $Co(hfac)_2$(PyrNN) has one crystallographically-independent cobalt(II) center and crystallizes in the $P2_1/c$ space group, which generates one unique chain with a 2_1 screw axis that extends along the chain direction; the easy axes of alternate chains are predicted to be antiparallel to each other in this compound (Figure S38). Compounds **3** and **4** both exhibit one crystallographically independent cobalt(II) center and a 2_1 screw axis along the chain direction, but the presence of a second perpendicular 2_1 screw axis defined by the $P2_12_12_1$ space group results in two different spatial arrangements of alternating chains, referred to here as Co^A and Co^B (Figure S39). Although the experimental magnetic data suggest an interaction between neighboring chains, their easy axes form an angle owing to the symmetry requirements of the crystal. In contrast to the single magnetic sublattice of $Co(hfac)_2$(PyrNN), two sublattices therefore exist for compounds **3** and **4**, which we hypothesize contribute to more complex magnetization processes for these compounds and their large coercivities. Indeed, the external field required for saturation of **3** and **4** as well as the coercive field are nearly double that of $Co(hfac)_2$(PyrNN).

We examine the proposed effect of two magnetic sublattices for **3** and **4** in more detail in Figure S40, based on the above magneto-structural analysis. At very low temperatures, in the absence of an external magnetic field, the magnetic moments of each sublattice are set along their easy axes and magnetically couple at thermal equilibrium (Figure S40a)—likely via dipolar interactions mediated by the close spacing between adjacent chains.[5c] Upon application of a field, the moments along the chain of one sublattice start to align with the field (Figure S40b), and with a still increasing external field, compound **3** or **4** will eventually reach its saturation magnetization M_s (Figure S40c). When the external field begins to decrease, the moments of each Co^A (or Co^B) chain relax and experience an additional (dipolar) magnetic field, H′, from the neighboring Co^B (or Co^A) chain that impedes demagnetization (Figure S40d) until the applied field in the opposite direction is strong enough to overcome these internal fields and force the moments to oppose each other at H_c (Figure S40e). As the reverse applied field continues to increase, the compound eventually saturates again in the opposite direction (Figure S40f). When the external field again reverses direction, the same demagnetization-magnetization process is repeated as described above (Figures S40g−i). The full process leading to formation of the hysteresis loop as described here is also depicted in Movie S1. Thus, in conjunction with the presence of strong magnetic interactions at low temperature, we propose that a physical property such as the existence of two canted sublattices can impede spin reversal and lead to remarkably large coercive fields. We emphasize here that, while previous experimental and theoretical studies of cobalt(II)–radical chain compounds have identified the role of three-dimensional ordering in generating large magnetic hysteresis,[7b,7c,11,12,15] our results demonstrate for the first time the pivotal role of the individual cobalt(II)–radical chain orientations in promoting magnetic hardness and reveal that *three-dimensional ordering is not a prerequisite for large coercivity*—while compound **3** exhibits evidence of long-range magnetic ordering below ~46.5 K, no such ordering is seen for **4**.

Conclusion

We have described the preparation of two discrete cobalt(II)–radical molecules $Co(hfac)_2$(R-NapNIT)$_2$ (R = MeO (**1**) and EtO (**2**)) and the corresponding chain compounds $Co(hfac)_2$(MeO-NapNIT) (**3**) and $Co(hfac)_2$(EtO-NapNIT) (**4**). While **1** and **2** behave as simple paramagnets, **3** and **4** behave as single-chain magnets and exhibit magnetization reversal barriers of 251±2 and 254±2 cm^{-1}, respectively, among the highest reported to date for any single-chain magnet. Both **3** and **4** also exhibit large, square magnetic hysteresis with giant coercive fields of 62 and 65 kOe, respectively, at 7 K. Our detailed structural and physical analyses suggest that a key factor in the low-temperature hard magnet behavior is *not three-dimensional ordering*, *but the presence of two distinct magnetic sublattices resulting from unique alternating chain conformations in the crystal lattice.* Interestingly, the angle between the easy axes of the cobalt(II) sites within the magnetic sublattices is larger for compound **4** than for **3** (31.48 versus 26.34°), and compound **4** exhibits a larger coercive field, which is needed to compensate the magnetic moments of its individual sublattices. These

differences between **3** and **4** can be correlated with the size of their radical ligand substituent, and it will therefore be interesting to explore ligand variants with even larger functional groups to confirm and investigate these magneto-structural correlations in greater detail. Future efforts will focus on extending this system to other anisotropic transition metal ions and related bridging radicals with different substituents to achieve even stronger magnetic exchange and, importantly, more fine-tuned control over the spatial arrangement of the individual chains, with the goal of accessing compounds exhibiting even higher coercive fields. Indeed, we believe that the concept of tuning the spatial arrangement of magnetic building units (chains in this work) may ultimately result in new high-performance magnets.

Acknowledgements

This research was funded by the National Key R&D Program of China (grant ref: 2018YFA0306002), the National Natural Science Foundation of China (grant refs: 21971123, 21622105 and 21861130354), the National Natural Science Foundation of Tianjin (grant ref: 18JCJQJC47200) and the Ministry of Education of China (grant ref: B12015). W. S. gratefully acknowledges the support of the Royal Society through a Newton Advanced Fellowship. The contributions of X.F., K.R.M., and J.R.L. were supported by NSF Grant CHE-1464841. We gratefully acknowledge Dr. Duming Wang (Quantum Design China) for collecting magnetic hysteresis using a high-field SQUID PPMS, Prof. Bing-Wu Wang (Peking University) for collecting heat capacity data, Prof. Kasper S. Pedersen (Technical University of Denmark) and Dr. Lukas Keller (Paul Scherrer Institute) for collecting powder neutron diffraction data, Prof. Zhengcai Xia (Wuhan National high Magnetic Field Center) for collecting hysteresis loops using a pulsed high magnetic field, Prof. Chuanying Xi and Prof. Li Pi (High Magnetic Field Laboratory, Chinese Academy of Sciences) for collecting hysteresis loops using a continuous high magnetic field.

Keywords: Magnetism • molecular magnetism • single-chain magnet • magnetic hysteresis • coercive field

[1] D. C. Jiles, *Introduction to Magnetism and Magnetic Materials*, Apple Academic Press Inc., Oakville, **2015**.

[2] a) M. S. Walmer, C. Chen, *IEEE Trans.* **2000**, *36*, 3376–3381; b) T. Kawai, B. Ma, S. G. Sankar, W. E. Wallace, *J. Appl. Phys.* **1990**, *67*, 4610–4612; c) R. Kütterer, H.-R. Hilzinger, H. Kronmüller, *J. Magn. Magn. Mater*.**1977**, *4*, 1–7.

[3] a) K. M. Krishnan, *Fundamentals and Applications of Magnetic Materials*, Oxford University Press, New York, **2016**; b) S. M. Girvin, K. Yang, *Modern Condensed Matter Physics*, Cambridge University Press, **2019**.

[4] a) R. Sessoli, D. Gatteschi, A. Caneschi, M. A. Novak, *Nature* **1993**, *365*, 141–143; b) R. A. Layfield, M. Muralee, *Lanthanides and Actinides in Molecular Magnetism*, Wiley-VCH, Weinheim, **2015**.

[5] a) A. Caneschi, D. Gatteschi, N. Lalioti, C. Sangregorio, R. Sessoli, G. Venturi, A. Vindigni, A. Rettori, M. G. Pini, M. A. Novak, *Angew. Chem., Int. Ed*. **2001**, *40*, 1760–1763; b) R. Clérac, H. Miyasaka, M. Yamashita, C. Coulon, *J. Am. Chem. Soc.* **2002**, *124*, 12837–12844; c) C. Coulon, H. Miyasaka, R. Clérac, *Single-Chain Magnets: Theoretical Approach and Experimental Systems. In Single-Molecule Magnets and Related Phenomena*, R. Winpenny, ed. Springer-Verlag Berlin Heidelberg, **2006**, pp. 164–206.

[6] a) R. J. Blagg, L. Ungur, F. Tuna, J. Speak, P. Comar, D. Collison, W. Wernsdorfer, E. J. L. McInnes, L. F. Chibotaru, R. E. P. Winpenny, *Nat. Chem.* **2013**, *5*, 673–678; b) J. Liu, Y.-C. Chen, J.-L. Liu, V. Vieru, L. Ungur, J.-H. Jia, L. F. Chibotaru, Y.-H. Lan, W. Wernsdorfer, S. Gao, X.-M. Chen, M.-L. Tong, *J. Am. Chem. Soc*. **2016**, *138*, 5441–5450; c) S. Demir, M. I. Gonzalez, L. E. Darago, J. R. Long, *Nat. Commun.* **2017**, 8, *2144*–2153; d) C. A. P. Goodwin, F. Ortu, D. Reta, N. F. Chilton, D. P. Mills, *Nature* **2017**, *548*, 439–442; e) F.-S. Guo, B. M.Day, Y.-C. Chen, M.-L. Tong, A. Mansikkamäki, R. A. Layfield, *Science* **2018**, *362*, 1400–1403.

[7] a) J. A. DeGayner, K. Y. Wang, T. D. Harris, *J. Am. Chem. Soc*. **2018**, *140*, 6550–6553; b) N. Ishii, Y. Okamura, S. Chiba, T. Nogami, T. Ishida, *J. Am. Chem. Soc*. **2008**, *130*, 24–25; c) M. G. F. Vaz, R. A. A. Cassaro, H. Akpinar, J. A. Schlueter, P. M. Lahti, M. A. Novak, *Chem. Eur. J*. **2014** *20*, 5460–5467.

[8] R. J. Glauber, *J. Math. Phys*. **1963**, *4*, 294–307.

[9] a) W. X. Zhang, R. Ishikawa, B. Breedlove, M. Yamashita, *RSC Adv*. **2013**, *3*, 3772–3798; b) X. Meng, W. Shi, P. Cheng, *Coord. Chem. Rev*. **2019**, *378*, 134–150.

[10] C. Coulon, R. Clérac, W. Wernsdorfer, T. Colin, H. Miyasaka, *Phys. Rev. Lett.* **2009**, *102*, 167204–.

[11] Y. Okamura, N. Ishii, T. Nogami, T. Ishida, *Bull. Chem. Soc. Jpn*. **2010**, *83*, 716–725.

[12] Y. Okamura, N. Ishii, T. Nogami, T. Ishida, *Chem. Lett*. **2009**, *38*, 740–741.

[13] Y. Numata, K. Inoue, N. Baranov, M. Kurmoo, K. Kikuchi, *J. Am. Chem. Soc*. **2007**, *129*, 9902–9909.

[14] R. Sessoli, *Angew. Chem., Int. Ed*. **2008**, *47*, 5508–5510.

[15] A. A. Bukharov, A. S. Ovchinnikov, N. V. Baranov, K. Inoue, *J. Phys. Condens. Matter* **2010**, *22*, 436003–436012.

[16] G. A. Craig, M. Murrie, *Chem. Soc. Rev*. **2015**, *44*, 2135–2147.

[17] N. F. Chilton, R. P. Anderson, L. D. Turner, A. Soncini, K. S. Murray, *J. Comput. Chem*. **2013**, *34*, 1164–1175.

[18] S. Stoll, A. Schmweiger, *J. Magn. Reson*. **2006,** *178*, 42–55; b) G. F. V. Maria, R. A. A. Cassaro, H. Akpinar, J. A. Schlueter, S. Jr. Santos, P. M. Lahti, M. A. Novak, *Inorg. Chem*. **2012**, *51*, 3138–3145.

[19] P. J. V. Koningsbruggen, O. Kahn, K. Nakatani, Y. Pei, J. P. Renard, Marc. Drillon, P. Legoll, *Inorg. Chem*. **1990**, *29*, 3325–3331.

[20] K. S. Pedersen, A. Vindigni, R. Sessoli, C. Coulon, R. Clérac, Single-Chain Magnets. In Molecular Magnetic Materials: Concepts and Applications, B. Sieklucka, D. Pinkowicz, eds. Wiley-VCH Verlag GmbH & Co. KGaA, New Jersey, **2017**, pp. 131‑161.

[21] J. A. Mydosh, Spin Glasses: An Experimental Introduction, Taylor & Francis, London, **1993**.

[22] S. Dhers, H. L. C. Feltham, S. Brooker, *Coord. Chem. Rev*. **2015**, *296*, 24–44.

[23] L.C lark, G. Sala, D. D. Maharaj, M. B. Stone, K. S. Knight, M. T. F. Telling, X. Y. Wang, X. H. Xu, J. Kim, Y. B. Li, S.-W. Cheong, B. D. Gaulin, *Nat. Phys*. **2019**, *15*, 262–268.

[24] O. Mustonen, S. Vasala, E. Sadrollahi, K. P. Schmidt, C. Baines, H. C. Walker, I. Terasaki, F. J. Litterst, E. Baggio-Saitovitch, M. Karppinen, *Nat. Commun*. **2018**, *9*, 1085–1093.

[25] S.-I. Ohkoshi, K. Imoto, A. Namai, S. Anan, M. Yoshikiyo, H. Tokoro, *J. Am. Chem. Soc*. **2017**, *139*, 13268–13271.

[26] a) P. Zhang, M. Perfetti, M. Kern, P. P. Hallmen, L. Ungur, S. Lenz, M. R. Ringenberg, W. Frey, H. Stoll, G. Rauhutf, J. van Slageren, *Chem. Sci*. **2018**, *9*, 1221–1230; b) L. F. Chibotaru, L. Ungur, *J. Chem. Phys.* **2012**, *137*, 064112.

[27] E. F. Ullman, J. H. Osiecki, D. G. B. Boocock, R. Darcy, *J. Am. Chem. Soc*. **1972**, *94*, 7049–7059.

Entry for the Table of Contents

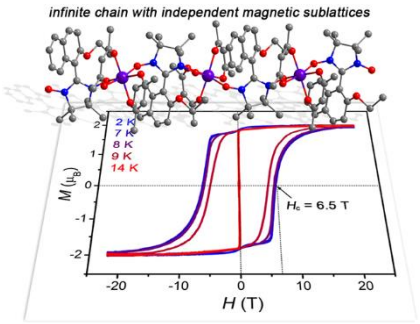

High-coercivity one-dimensional magnets: novel cobalt(II)–nitronyl nitroxide radical chains featuring crystallographically-determined alternating magnetic sublattices exhibit exceptional magnetic hardness and coercive fields up to 65 kOe.